Available online at www.sciencedirect.com

ScienceDirect

Advances in Space Research 67 (2021) 4089–4098

ADVANCES IN SPACE RESEARCH (a COSPAR publication)

www.elsevier.com/locate/asr

The Kumtag meteorite strewn field

Ke Du [a,b], Shijie Li [a,c,*], Ingo Leya [d], Thomas Smith [d,e], Dongliang Zhang [f], Peng Wang [g]

[a] Center for Lunar and Planetary Sciences, Institute of Geochemistry, Chinese Academy of Sciences, Guiyang 550081, China
[b] University of Chinese Academy of Sciences, Beijing 100049, China
[c] Chinese Academy of Sciences Center for Excellence in Comparative Planetology, Hefei 230026, China
[d] Physics Institute, University of Bern, CH-3012 Bern, Switzerland
[e] State Key Laboratory of Lithospheric Evolution, Institute of Geology and Geophysics, Chinese Academy of Sciences, 100029 Beijing, China
[f] Key Laboratory of Metallogenic Prediction of Nonferrous Metals, Ministry of Education, School of Geosciences and Info-physics, Central South University, Changsha 410083, China
[g] Division of Mines and Geology, Sixth Geological Brigade, Hami 839000, China

Received 14 October 2020; received in revised form 7 January 2021; accepted 13 February 2021
Available online 24 February 2021

Abstract

The Kumtag meteorite strewn field was found in the Kumtag desert, 132 km south of Hami city in the Xinjiang province, China. It is an ellipse of 2.5 × 7.9 km, with a long axis extending along the northeast-southwest direction. The largest individual meteorite of the strewn field weighs about 10 kg; the smallest individual has a mass of only 27 g. In total, more than 100 individuals with a total mass of more than 180 kg were collected. The location and the distribution of the fragments suggest that the Kumtag meteoroid entered the atmosphere in the direction Northeast-Southwest. All meteorites collected in this strewn field are samples from the same unique meteorite shower. The Kumtag meteorite is an H5 ordinary chondrite with a shock stage S2, and a weathering grade W2. The cosmic ray exposure age of Kumtag is 6.7 ± 0.8 Ma, which is rather typical for H chondrites and which indicates that Kumtag was derived from the massive impact event on its parent body ~7 Ma ago. A significant amount of He has been lost during certain unknown processe(s) before the Kumtag meteorite was ejected from its parent body.

Keywords: Kumtag desert; Strewn field; Chondrite meteorite; Cosmic-ray exposure age

1. Introduction

A meteorite is an extraterrestrial rock surviving its fall through the Earth atmosphere, which can provide crucial information about the early solar system but also about the dynamics of small bodies in the solar system. To date, meteorites found in Antarctica represent 55% of all meteorites in our collections (Meteoritical Bulletin Database (MBD)), the other collected meteorites are mainly from hot deserts. Compared to the sometimes difficult meteorite search expeditions in Antarctica, more and more meteorite hunters prefer to search for meteorites in hot deserts due to the advantages of low costs, relatively low risks, and relatively comfortable working environments. To date, a large number of meteorites are found in many hot deserts worldwide. The regions include the Atacama (Muñoz et al., 2007;

Abbreviations: MBD, Meteoritical Bulletin Database; ASL, above sea level; BSE, backscattered electron; Fa, fayalite; Fs, ferrosilite; CRE, cosmic-ray exposure

* Corresponding author at: Center for Lunar and Planetary Sciences, Institute of Geochemistry, Chinese Academy of Sciences, Guiyang 550081, China.
E-mail address: lishijielpsc@mail.gyig.ac.cn (S. Li).

https://doi.org/10.1016/j.asr.2021.02.020
0273-1177/

Gattacceca et al., 2011; Hutzler et al., 2016), Sahara (Bischoff and Geiger, 1995; Schluter et al., 2002; Ouazaa et al., 2009), Southwestern United States (Zolensky et al., 1990; Rubin et al., 2000; Kring et al., 2001; Hutson et al., 2013), the Lut Desert in Iran (Pourkhorsandi and Mirnejad, 2013; Pourkhorsandi et al., 2019), and the Xinjiang Province in China (Li and Hsu, 2014; Li et al. 2017; Zeng et al., 2018). Although large number meteorites from hot deserts have been studied over the years, there are only very few studies of meteorites from Chinese hot deserts (Li et al. 2017; Zeng et al. 2018).

The Kumtag meteorite strewn field is located east of the Kumtag sand levee, which is 132 km from Hami city, Xinjiang, China. The strewn field is almost an ellipse, with its long axis extending from northeast to southwest. After its first discovery in 2008, more than 150 individual meteorites with a total mass of more than 180 kg have been collected during more than 20 successive meteorite searching campaigns. All individuals are named Kumtag in the Meteoritical Bulletin Database (MBD).

Here we present and discuss the physical geographic features and the geological background of the strewn field and we will mention the process of meteorite search. Furthermore, we will report the petrological characteristics and the cosmic ray exposure (CRE) ages of representative meteorites from this strewn field. In addition, we will give the gas retention age and the preatmospheric size.

2. Geographical features and geological background of the strewn field

The area of the meteorite strewn field is characterized by harsh natural conditions, including extreme droughts, a complex geomorphology, and diverse dune types, especially the unique feather dune. The elevation of the strewn field is between 1130 and 1190 m above sea level (ASL), the average elevation is about 1170 m ASL, and the change in altitude across the strewn field is about 20–60 m. The area of the Kumtag meteorite strewn field is in the inland arid region, where the average annual temperature ranges from more than 40 °C at the high end down to −30 °C at the low end. The Kumtag desert is far away from the ocean, therefore only very little water vapor can reach the desert from the warm and wet air originating from the Pacific Ocean. From the other side, the Qinghai-Tibetan Plateau acts as a natural barrier, only a small part of the water vapor from Indian Ocean can cross the Hengduan Mountains. The area of Kumtag is extremely arid with an average annual precipitation of not more than 25 mm. The average annual evaporation is higher than 3000 mm and the relative humidity is between 35% and 43% (Yang et al., 2012).

In this strewn-field area magmatic rocks are widely exposed (Fig. 1a); the most widely exposed rocks are gray-white and light-red granites formed in the Variscan period (Zhang et al., 2010). Other, intrusive rocks, in this field mostly consist of norite gabbro, grey-green gabbro, and quartz diorite, which were formed in the early Variscan period (prior the intrusion of granite) (Zhang et al., 2010). The surface rock is severely weathered and has been broken into sand and centimeter-sized rubble (Fig. 1b, c). The lower terrain is often covered with a thin layer of sands (Fig. 1d).

3. Meteorite distribution in the strewn field

The first meteorite in this strewn field was accidentally found by one of coauthors (Peng Wang) on October 9, 2008, during his geological field work. A piece of a fractured black rock was collected on a granite pluton. After being broken with a geological hammer, silver white metal spots were observed on the fresh broken surface of this rock and it has therefore been identified as a possible meteorite. A piece of the meteorite with a mass of 969 g was donated to the Purple Mountain Observatory, Chinese Academy of Sciences in 2009. This piece was later named Kumtag (H5) by the Meteorite Nomenclature Committee. In the next eight years, about 130 meteorites have been collected by Peng Wang and his team of geologists in search campaigns either by foot or using cars. Among these meteorites, the GPS coordinates of 95 of them are known. In addition, the coordinates of more than 40 kg of specimens are not known or have not been recorded because they have been collected by other meteorite hunters in this field.

According to the GPS coordinates, meteorites collected east of the Kumtag sand levee cover approximately an ellipse with dimensions 2.5 × 7.9 km, with a long axis extending from the northeast to the southwest (Fig. 2). In addition, meteorite sizes gradually increase along the long axis (northeast – southwest orientation). Meteorites collected near the northeast edge are usually less than 500 g in weight, while samples from the southwest edge are usually over 1 kg in mass. The largest individual (11.05 kg) was collected at the southwest border of this elliptical area. The study of the Jilin meteorite and other meteorite strewn fields demonstrate that the largest fragments have the longest flightpath, i.e., it indicates the upper end of the strewn field, and usually there is a size-sorting of fragments, i.e., the smallest fragment falls earliest (Joint investigation group of "Jilin meteorite shower", 1977; Simon et al., 2004; Gnos et al., 2009; Li et al., 2017; Zeng et al., 2018; Li et al., 2020). The location and the distribution of the fragments definitely suggest that (1) this collection area is a meteorite strewn field and (2) the entry direction of the Kumtag parent meteorite into the Earth atmosphere was from the northeast to the southwest (Fig. 2).

In addition, the Kumtag 049 meteorite found close to this strewn field is not part of this meteorite shower. Kumtag 049 is a L group meteorite (MBD) which has been found about 2 km away from the nearest strewn field samples (see Fig. 2).

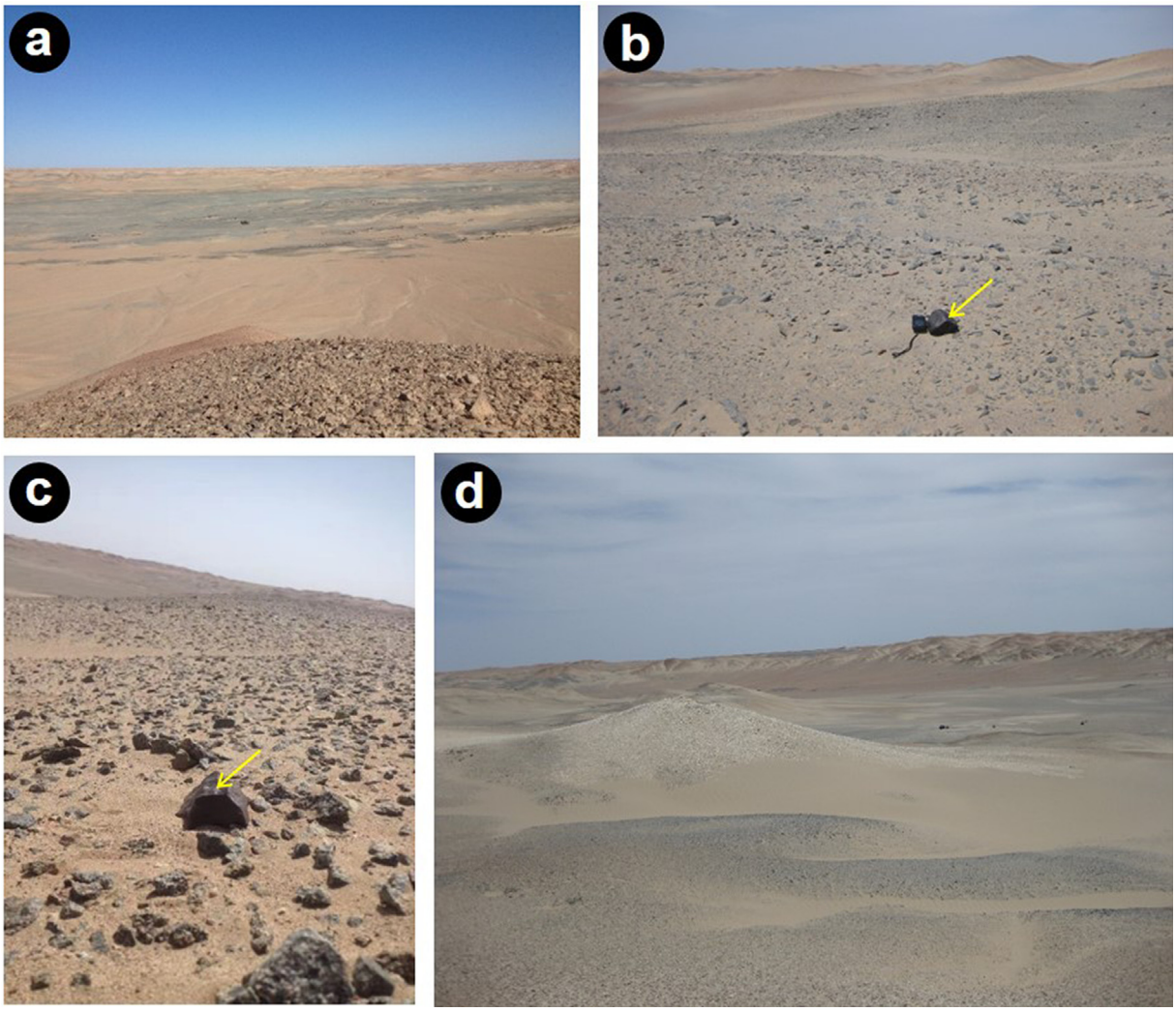

Fig. 1. Surface features of the Kumtag meteorite collection area. (a) The meteorite collection area consists of granite (reddish) and gabbro (dark areas); (b, c) The surface is covered with the mixture of gravel and sand. The lower right of panel (b) shows a meteorite (indicated by the arrow), a GPS at the left of the meteorite severs as a scale. The black rock shown in the middle of panel (c) is also a meteorite (indicated by the arrow). (d) The lower part of the meteorite strewn field is covered with a thin layer of sand.

4. Samples and methods

In this study, eight meteorites (labeled Kumtag-2 - Kumtag-9) from the strewn field were selected for petrographic studies and mineral in situ chemical analysis. One sample was selected for measurements of the isotopic concentrations of the light noble gases (He, Ne, and Ar). One sample (Kumtag-7) was mounted on a thin section with standard thickness (~0.03 mm) for assessing the shock stage under the polarized light microscopy. The petrographic investigations and the backscattered electron (BSE) images were performed at the Lunar and Planetary Science Research Center, Institute of Geochemistry, Chinese Academy of Sciences, using an FEI-Scios Field Emission Scanning Electron Microscope (FE-SEM). The instrument was operated at an acceleration voltage of 15–20 kV, a beam current of 3.2–6.4 nA, and a working distance of 7–10 mm. The electron microprobe analysis of olivine and low-calcium pyroxene was carried out at the Guilin University of Technology. The instrument used was a JXA 8230 electron probe, the analysis voltage was 15 kV, the beam current was 20 nA, and the beam spot diameter was 1 μm. The analysis results were corrected using the ZAF method. The noble gas isotopic concentrations were measured using two self-made noble gas mass spectrometers at the University of Bern, Switzerland, following the procedure previously described by Li et al. (2017).

5. Results and discussion

5.1. The appearance and petrology of meteorites

Kumtag meteorites show various surface characteristics. Some stones are completely covered with black fusion crust

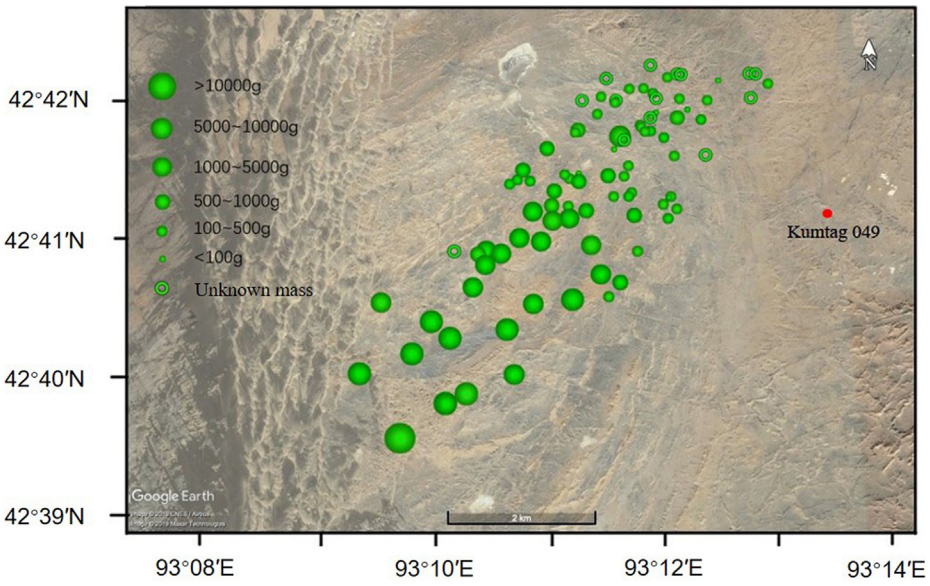

Fig. 2. Map of the Kumtag meteorites strewn field (Kumtag desert, Xinjiang Province, China). The green circles represent the meteorites found in the strewn field. The position of the (unpaired) L group meteorite Kumtag 049 (the red solid spot) is also shown. (The base map is from Google Earth). (For interpretation of the references to colour in this figure legend, the reader is referred to the web version of this article.)

and show well developed regmaglypts (Fig. 3a). Part of the meteorites in contact with the desert sand are often covered with rust (Fig. 3b), which was formed during terrestrial weathering. Note that the rusty spot on the ground-touching surface is very often a strong indicator for hot-desert meteorites, especially for relatively iron-rich ordinary chondrites, particularly from the H group. The largest meteorite of the strewn field with a mass of 10.05 kg is shown in Fig. 3c. This individual is only covered with fusion crust and regmaglypts on one side; the broken surface indicates the meteorite fragment was even bigger (Fig. 3c). Highly fractured meteorites were also collected; their cracks were often partially filled with sand (Fig. 3d). In hot desert environments, meteorites often break into dozens of pieces during their landing and/or during terrestrial weathering (Fig. 3e). Two meteorites with a secondary fusion crust were collected. It is obvious, based on their geometry, that these two objects came from one single fragment of the meteorite shower (Fig. 3f).

The eight studied Kumtag meteorite samples have similar mineral composition, shock characteristics, and weathering grade. The meteorites are mainly composed of olivine, pyroxene, plagioclase, Fe-Ni metal, troilite, and some weathering products (Fig. 4). Texturally, the boundaries of the chondrules are vague but distinct. The plagioclase grain size is mostly between 2 and 50 μm. The modal abundance of Fe-Ni metal in these meteorites is about 7 vol%. Fe-Ni metal in meteorites have irregular shapes, with grain sizes ranging from 50 to 200 μm, which usually occurs between silicate grains. In addition, some small Fe-Ni metal particles are scattered sporadically in the matrix. Consequently, Kumtag is a type 5 chondrite (Van Schmus and Wood, 1967). The average fayalite (Fa) content of olivines and the average ferrosilite (Fs) content of the low-Ca pyroxenes are 18.50 ± 0.31 mol% and 16.60 ± 0.69 mol% (Table 1), respectively, clearly indicating that Kumtag is a H chondrite (Brearley and Jones, 1998; Weisberg et al., 2006). On the polished section and under the electron microscope most of the olivine grains show irregular fractures and wavy edges. No melt vein has been observed in the studied sections, which suggests that the meteorites suffered relatively weak shock. The olivine and plagioclase grains show irregular fractures and undulatory extinction under the polarized light, consistent with a shock stage of S2 (Stoffler et al., 1991). In the studied sections, about 25 vol% of the Fe-Ni metal has been replaced by weathering products, indicating a weathering degree W2 (Wlotzka, 1993).

5.2. Cosmic-ray exposure ages, preatmospheric size, and gas retention ages

The concentrations and isotopic ratios of the light noble gases He, Ne, and Ar were measured in one Kumtag meteorite. The results, corrected for blank contributions and instrumental mass fractionation, are shown in Table 2. For the component deconvolution, we assume that the measured Ne and Ar concentrations are mixtures between cosmogenic (“c”) and trapped components, the latter being atmospheric contamination (“air”). Note that atmospheric contamination is very common for hot desert, weathered meteorites (e.g., Huber et al., 2006). For calculating $^{21}Ne_c$ and $^{38}Ar_c$ via the component deconvolution we use the following endmembers: ($^{20}Ne/^{22}$-

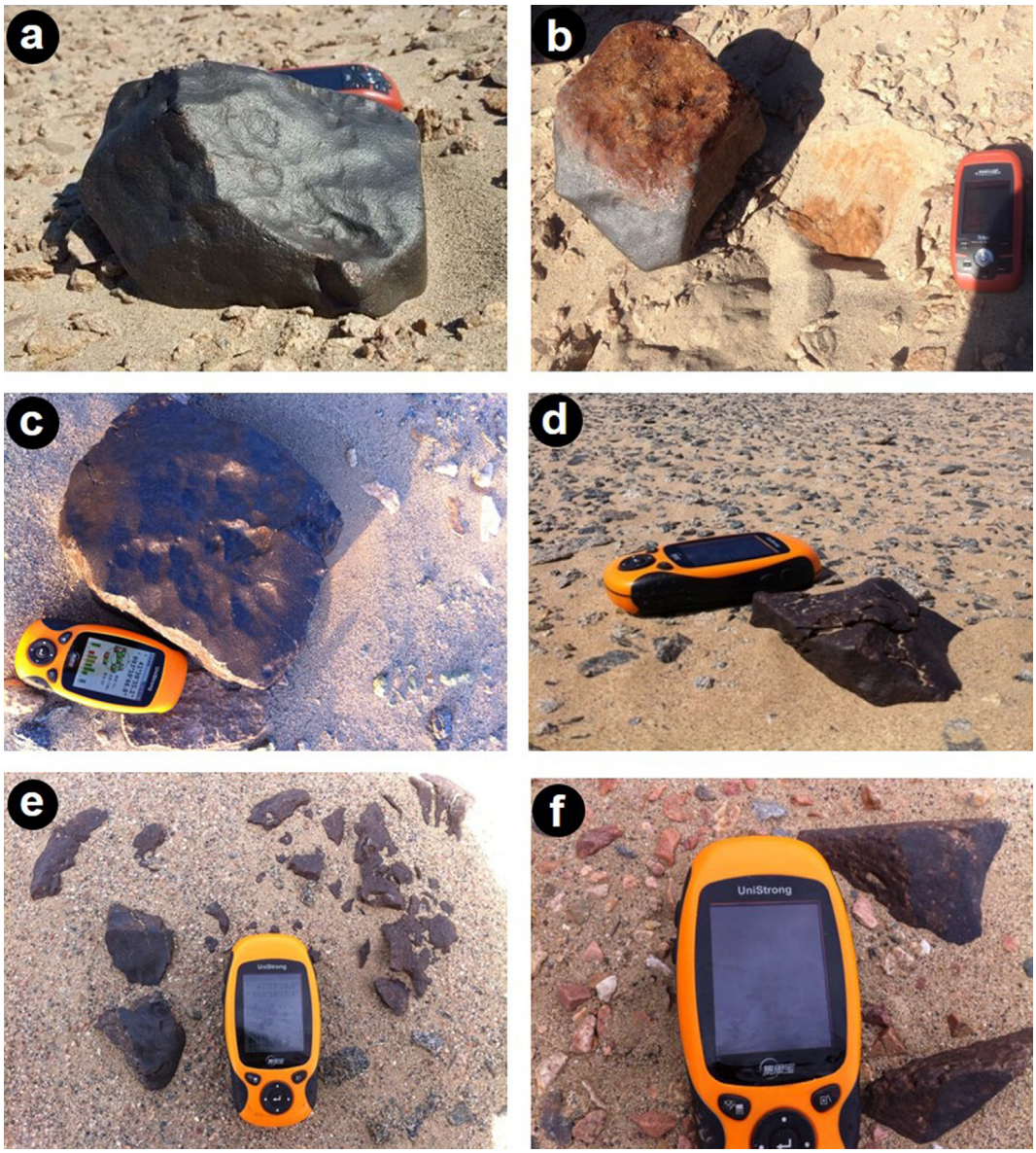

Fig. 3. Photographs of the selected Kumtag meteorites. (a, b) A single meteorite having a mass of 7470 g. Panel (a) shows the surface with black fusion crust and well developed regmaglypts. Panel (b) shows the surface buried in the desert. (c) A 10.05 kg meteorite with brown-black surface and fusion crust. (d, e) Broken meteorites in the strewn field. (f) Two meteorites that are part of the same fragment showing secondary fusion crust.

$Ne)_c = 0.84$, $(^{36}Ar/^{38}Ar)_c = 0.65$, $(^{20}Ne/^{22}Ne)_{air} = 9.80$, $(^{21}Ne/^{22}Ne)_{air} = 0.029$, and $(^{36}Ar/^{38}Ar)_{air} = 5.35$ (Eberhardt et al., 1965; Lee et al., 2006). Note that the cosmogenic endmember composition $(^{20}Ne/^{22}Ne)_c = 0.84$ corresponds to the measured ratio, which clearly indicates that the amount of atmospheric contamination for Ne isotopes is only very minor. We further assume that the measured ^3He concentration is entirely cosmogenic. The thus calculated cosmogenic $^{21}Ne_c$ and $^{38}Ar_c$ concentrations are given in Table 3. The production rates were calculated using the model by Eugster (1988) and the cosmic-ray exposure (CRE) ages are given in Table 4. The CRE ages T_3, T_{21}, and T_{38}, based on ^3He_c, $^{21}Ne_c$, and $^{38}Ar_c$ concentrations, respectively, of the Kumtag meteorite are 6.3 ± 1.9 Ma, 6.2 ± 1.9 Ma, and 7.7 ± 2.4 Ma, respectively. The grand average CRE age is 6.7 ± 0.8 M a, which represents the CRE age of the Kumtag strewn field meteorite. The weathering degree of the Kumtag strewn field is W2, indicating a relatively short terrestrial age. From this finding it is therefore safe to assume that the CRE age of Kumtag is very close to the ejection age, i.e., 6.7 ± 0.8 Ma. The thus determined CRE (or ejection) age is consistent with typical CRE ages for other H chondrites, which have a peak centered at about 7 Ma in

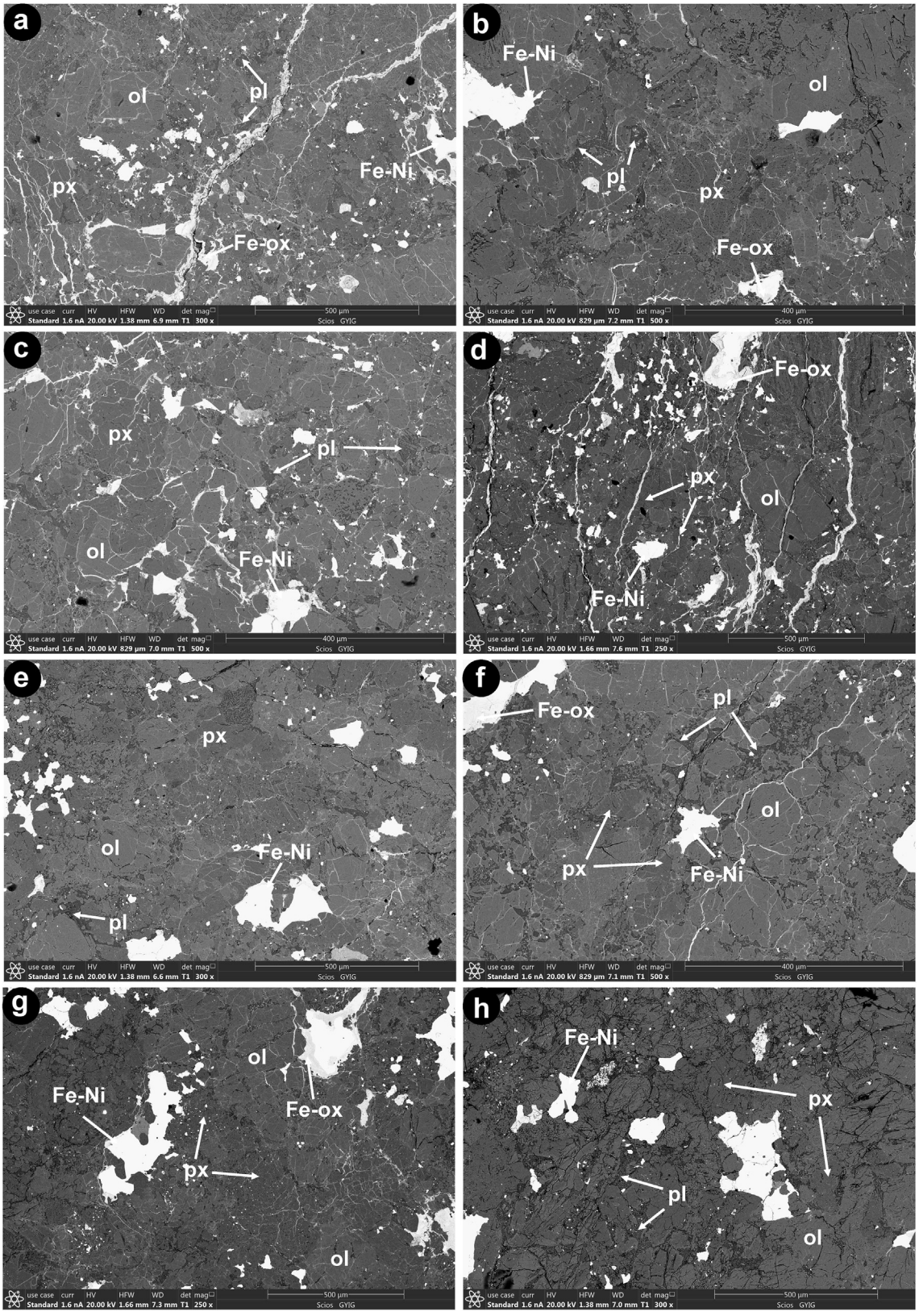

Fig. 4. Backscattered electron images of Kumtag. Panels a–h show the images for Kumtag-2 to Kumtag-9, respectively. The visible minerals include olivine, pyroxene, plagioclase, and veinlets filled with iron oxide. The Fe-Ni metal has been partially replaced by weathering products. The labeled minerals include olivine (ol), pyroxene (px), plagioclase (pl), and Fe-oxides (Fe-ox).

Table 1
The average electron probe analysis results of olivine (Ol, n = 2 for each individual meteorite) and pyroxene (Pyx, n = 2 for each individual meteorite) in Kumtag meteorite. The detection limit is about 0.04 wt%, values lower than this is listed as <0.04 wt%. The uncertainties are 1SD, Ol represents olivine and Pyx represents pyroxene.

Sample	mineral	Na_2O	MgO	Al_2O_3	K_2O	FeO	MnO	TiO_2	CaO	NiO	Cr_2O_3	SiO_2	Total	Fa/Fs
Kumtag-2	Ol	<0.04	29.6 ± 0.9	0.16 ± 0.02	<0.04	10.8 ± 0.1	1.16 ± 0.07	0.41 ± 0.18	0.84 ± 0.03	0.05 ± 0.07	0.19 ± 0.05	56.1 ± 1.2	99.4 ± 0.4	18.6 ± 0.3
	Pyx	<0.04	42.0 ± 0.9	<0.04	<0.04	17.2 ± 0.5	1.06 ± 0.10	0.07 ± 0.09	<0.04	<0.04	<0.04	39.1 ± 0.6	99.6 ± 0.9	16.9 ± 0.3
Kumtag-3	Ol	<0.04	29.9 ± 1.9	0.12 ± 0.03	<0.04	10.8 ± 0.2	1.15 ± 0.30	0.06 ± 0.06	0.53 ± 0.29	<0.04	0.13 ± 0.01	55.6 ± 1.6	98.5 ± 0.6	18.3 ± 0.2
	Pyx	<0.04	43.2 ± 0.4	<0.04	<0.04	17.2 ± 0.1	1.13 ± 0.04	0.06 ± 0.03	<0.04	<0.04	<0.04	38.2 ± 0.1	100.0 ± 0.3	16.4 ± 0.6
Kumtag-4	Ol	<0.04	30.3 ± 0.1	0.30 ± 0.15	<0.04	11.3 ± 0.5	1.08 ± 0.11	0.59 ± 0.18	0.78 ± 0.01	<0.04	0.23 ± 0.14	54.4 ± 0.9	99.0 ± 1.1	18.5 ± 0.3
	Pyx	<0.04	42.6 ± 1.1	<0.04	<0.04	17.2 ± 0.1	0.99 ± 0.16	0.14 ± 0.07	<0.04	<0.04	<0.04	37.6 ± 0.5	98.6 ± 0.5	16.9 ± 0.7
Kumtag-5	Ol	<0.04	30.1 ± 0.6	0.21 ± 0.02	<0.04	11.0 ± 0.3	1.15 ± 0.13	0.39 ± 0.12	0.82 ± 0.01	<0.04	0.18 ± 0.03	55.1 ± 0.5	98.9 ± 0.7	18.7 ± 0.4
	Pyx	<0.04	42.3 ± 1.4	<0.04	<0.04	17.3 ± 0.2	1.09 ± 0.11	0.05 ± 0.10	<0.04	<0.04	<0.04	38.0 ± 0.9	98.9 ± 0.4	16.8 ± 0.1
Kumtag-6	Ol	<0.04	30.9 ± 0.1	0.15 ± 0.03	<0.04	11.4 ± 0.5	1.16 ± 0.04	0.14 ± 0.09	0.68 ± 0.03	<0.04	0.15 ± 0.01	53.9 ± 0.2	98.6 ± 0.7	18.5 ± 0.4
	Pyx	<0.04	42.4 ± 0.3	<0.04	<0.04	17.2 ± 0.4	1.01 ± 0.04	<0.04	<0.04	<0.04	<0.04	38.0 ± 0.40	98.7 ± 0.5	17.0 ± 0.6
Kumtag-7	Ol	<0.04	30.9 ± 0.01	0.26 ± 0.09	<0.04	10.7 ± 0.1	1.11 ± 0.15	0.59 ± 0.11	0.67 ± 0.13	<0.04	0.18 ± 0.10	55.3 ± 0.1	99.8 ± 0.6	18.5 ± 0.4
	Pyx	<0.04	42.8 ± 0.7	<0.04	<0.04	17.2 ± 0.3	0.95 ± 0.11	<0.04	<0.04	<0.04	<0.04	38.9 ± 0.6	100.0 ± 1.0	16.1 ± 0.1
Kumtag-8	Ol	<0.04	31.3 ± 0.6	0.26 ± 0.15	<0.04	10.9 ± 0.2	1.25 ± 0.09	0.45 ± 0.13	0.69 ± 0.03	<0.04	0.41 ± 0.35	53.2 ± 1.1	98.5 ± 0.7	18.5 ± 0.3
	Pyx	<0.04	42.8 ± 0.8	<0.04	<0.04	17.4 ± 0.2	0.93 ± 0.15	<0.04	<0.04	0.06 ± 0.07	<0.04	38.4 ± 0.4	99.7 ± 0.9	16.1 ± 0.5
Kumtag-9	Ol	<0.04	30.7 ± 0.8	0.11 ± 0.01	<0.04	11.2 ± 1.0	1.10 ± 0.09	0.11 ± 0.19	0.64 ± 0.19	0.06 ± 0.06	0.12 ± 0.01	55.8 ± 0.7	99.8 ± 0.8	18.5 ± 0.3
	Pyx	<0.04	43.0 ± 0.6	<0.04	<0.04	17.4 ± 0.4	1.11 ± 0.10	0.12 ± 0.10	<0.04	<0.04	<0.04	38.5 ± 0.7	100.2 ± 0.6	16.8 ± 1.5

the CRE age histogram (Herzog and Caffee, 2014). The preatmospheric size and the mass of a meteorite can be estimated using the cosmogenic $(^{22}Ne/^{21}Ne)_c$ ratio, which is a known indicator for shielding (Bhandari et al., 1980; Leya and Masarik, 2009). From the empirical equation given by Bhandari et al. (1980) and the determined $(^{22}Ne/^{21}Ne)_c$ ratio of 1.083 ± 0.017, we calculate a preatmospheric mass of 115.8 ± 32.6 kg, which is in contradiction to the total recovered mass of all Kumtag meteorites of >180 kg. Possibilities to account for such a difference are (i) Kumtag was not a spherical object and the effective radius was much smaller than the estimated radius, (ii) the correlation between $(^{22}Ne/^{21}Ne)_c$ and spherical size deduced from Bhandari et al. (1980) is not applicable for the Kumtag meteorite because this special sample might come from an outer layer of the meteorite. Note also that the correlation given by Bhandari et al. (1980) only gives a lower limit for the preatmospheric mass (Zeng et al., 2018). From the total recovered mass of ~180 kg, an average bulk density of 3.567 g/cm^3 (Li et al., 2019), and assuming an ablation loss of ~87% (Bhandari et al., 1980) we calculate a pre-atmospheric radius of ~45 cm.

To calculate the ^{4}He and ^{40}Ar gas retention ages of the Kumtag meteorite, we use the average U, Th, and K concentrations for H-group ordinary chondrites given by Lodders et al. (1998). The concentration of radiogenic component (^4He_r and $^{40}Ar_r$) has been determined by subtracting cosmogenic component (^4He_c and $^{40}Ar_c$) and trapped component ($^4He_{air}$ and $^{40}Ar_{air}$) contributions, note that the $^4He_{air}$ and $^{40}Ar_c$ components are negligible (Table 3). The thus determined gas retention ages are T_4 = 2508 Ma and T_{40} = 3908 Ma (Table 4), i.e., T_4 is significantly lower than T_{40}. Consequently, the Kumtag meteorite plots to the left of the solid line with slope 1 (Fig. 5). In this diagram, samples with identical CRE ages based on ^{3}He and ^{21}Ne plot close to 1 on the y-axis and samples with identical T_4 and T_{40} plot close to 1 on the x-axis. Samples that simultaneously lost ^{3}He and ^{4}He move along the line with slope 1. For the studied meteorite we have T_3/T_{21} = 1.02 ± 0.44 and T_4/T_{40} = 0.64 ± 0.06. The T_3/T_{21} ratio of 1.02 ± 0.44 suggests no or only minor losses of cosmogenic ^{3}He and/or ^{3}He. This finding is further confirmed when studying the data in a diagram $(^3He/^{21}Ne)_c$ vs. $(^{22}Ne/^{21}Ne)_c$, i.e., in the Bern-plot (Nishiizumi et al., 1980) (Fig. 6). Also, this data indicates no or only little losses of cosmogenic ^{3}He and/or ^{3}He.

In contrast, the ratio T_4/T_{40} of 0.64 ± 0.06 is significantly lower than 1, indicating loss of radiogenic ^4He_r. Since the ^{4}He loss is not accompanied by ^{3}He loss, it likely occurred before ejection of the Kumtag meteorite from the H chondrite parent body. The exact reason for the loss of radiogenic ^4He_r is unclear, but it might be connected to a severe heating generated from a huge impact event which occurred on the surrounding rocks of the parent body. The temperature generated by this event might have exceeded the closure temperature of He, which would have

Table 2
He, Ne, and Ar isotopic concentrations of the Kumtag meteorite (10^{-8} cm^3 STP g^{-1}).

Meteorite	Type	Mass (mg)	^{3}He	^{4}He	^{22}Ne	^{36}Ar	^{40}Ar	^{20}Ne/^{22}Ne	^{21}Ne/^{22}Ne	^{36}Ar/^{38}Ar
Kumtag	H5	71.33	10.1 ± 0.6	877 ± 48	2.61 ± 0.19	0.989 ± 0.034	4367 ± 76	0.846 ± 0.013	0.919 ± 0.014	1.88 ± 0.05

Table 3
Cosmogenic and radiogenic noble gases of the Kumtag meteorite (10^{-8} cm^3 STP g^{-1}). "c" and "r" represent cosmogenic and radiogenic nuclides components.

Meteorite	Type	Mass (mg)	^{3}He$_c$	^{21}Ne$_c$	^{38}Ar$_c$	(^{22}Ne/^{21}Ne)$_c$	^{4}He$_r$	^{40}Ar$_r$
Kumtag	H5	71.33	10.1 ± 0.6	2.40 ± 0.18	0.385 ± 0.027	1.083 ± 0.017	827 ± 48	4147 ± 72

Table 4
Cosmic-ray exposure ages and retention ages of the Kumtag meteorite (in Ma). The gas retention ages were calculated using average K, U, Th, and Sm concentrations for H ordinary chondrites (Lodders et al., 1998).

Meteorite	Type	Mass (mg)	T_3	T_{21}	T_{38}	Adopted age	T_4	T_{40}	T_3/T_{21}	T_4/T_{40}
Kumtag	H5	71.33	6.3 ± 1.9	6.2 ± 1.9	7.7 ± 2.4	6.7 ± 0.8	2508 ± 170	3908 ± 227	1.02 ± 0.44	0.64 ± 0.06

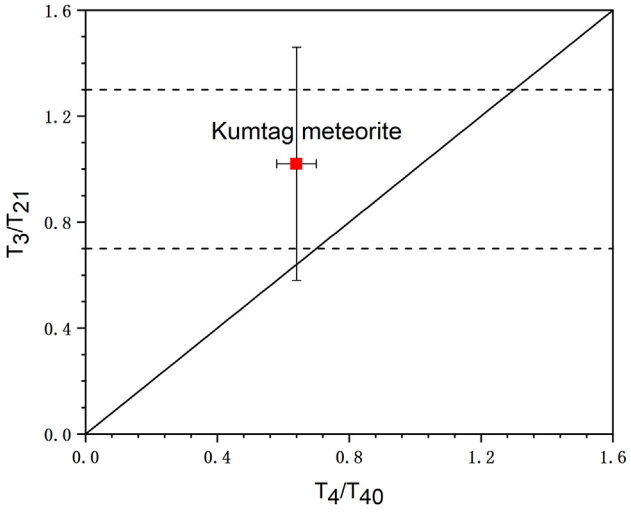

Fig. 5. Ratio of CRE ages (T_3/T_{21}) versus ratios of gas retention ages (T_4/T_{40}) for the studied Kumtag meteorite (red solid circle). T_3/T_{21}, ratios between the two dotted lines indicate that there is no ^{3}He deficit, which is very often due to ^{3}He and/or ^{3}He losses. The relatively low T_4/T_{40} ratio of the Kumtag meteorite indicates loss of radiogenic ^{4}He before its ejection from the parent body. (For interpretation of the references to colour in this figure legend, the reader is referred to the web version of this article.)

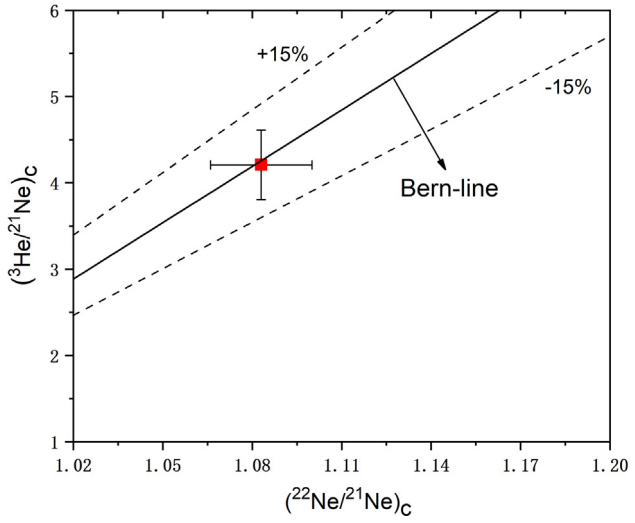

Fig. 6. The "Bern plot"- correlation of (^{3}He/^{21}Ne)$_c$ versus (^{22}Ne/^{21}Ne)$_c$ for the Kumtag meteorite (the red circle). The solid line is the best fit line given by Nishiizumi et al. (1980). The dashed lines represent the ±15% variations from this correlation. (For interpretation of the references to colour in this figure legend, the reader is referred to the web version of this article.)

led to the loss of ^{4}He$_r$. It is unlikely that the ^{4}He loss was caused by a direct shock event, because the studied Kumtag individual has a shock stage of only S2 (Stoffler et al., 1991). However, it cannot be excluded that the ^{4}He and/or ^{40}Ar gas retention age are too high or too low due to wrong assumptions about U, Th, and K concentrations.

6. Conclusions

The Kumtag meteorite strewn field has an elliptical shape with a long axis of about 7.9 km and a short axis of about 2.5 km. The Kumtag meteorite entered the atmosphere in a northeast-southwest direction. The meteorites collected in the Kumtag strewn field are typical H5 ordinary chondrites, which suffered relatively weak shock and

low weathering. Compared to most other desert meteorites, the Kumtag meteorites show a relatively low degree of weathering. This either suggests that the terrestrial ages of Kumtag is low and/or that the extremely dry conditions reduce weathering processes. Therefore, the CRE age of Kumtag is 6.7 ± 0.8 Ma, which is likely very close to the ejection age, assuming a short terrestrial age. The ^{3}He and ^{21}Ne CRE ages and ^{4}He and ^{40}Ar gas retention ages indicate that the material now forming the Kumtag meteorite likely lost radiogenic ^{4}He before ejection from the parent body.

Declaration of Competing Interest

The authors declare that they have no known competing financial interests or personal relationships that could have appeared to influence the work reported in this paper.

Acknowledgements

This work has been supported by the Strategic Priority Research Program of Chinese Academy of Sciences (Grant No. XDB 41000000) and the Chinese Academy of Sciences "Light of West China" Program (Shijie Li, 2019) and the Swiss National Science Foundations (IL: 200021_159562). We thank the FIB laboratory team at IGCAS for the SEM and BSE studies and Hans-Erich Jenni for his help during the noble gas measurements. Finally, we are grateful to Lanfang Xie for her support during EPMA measurement.

Availability of data and materials

The data and materials are available upon request from the first author Ke Du (e-mail: duke@mail.gyig.ac.cn).

Funding

This work has been supported by the Strategic Priority Research Program of Chinese Academy of Sciences (Grant No. XDB 41000000) and the Chinese Academy of Sciences "Light of West China" Program (Shijie Li, 2019) and the Swiss National Science Foundations (IL: 200021_159562).

Contributions

Ke Du prepared the paper draft. Shijie Li, Ingo Leya, Thomas Amith and Dongliang Zhang determined the noble gas data, and calculated the element ratios and CRE ages. Peng Wang collected and provided the samples. All authors participated in the discussion of results and contributed to the editing of the final manuscript. All authors read and approved the final manuscript.

References

Bischoff, A., Geiger, T., 1995. Meteorites from the Sahara: Find locations, shock classification, degree of weathering and pairing. Meteorit. Planet. Sci. 30, 113–122.

Bhandari, N., Lal, D., Rajan, R.S., Arnold, J.R., Marti, K., Moore, C.B., 1980. Atmospheric ablation in meteorites: A study based on cosmic ray tracks and neon isotopes. Nucl. Tracks 4, 213–262.

Brearley, A.J., Jones, R.H., 1998. Chondritic meteorites. In: Planetary Materials, edited by Papike J. J. Reviews in Mineralogy, vol. 36. Mineralogical Society of America, Washington, D.C., pp. 3-1–3-398.

Eberhardt, P., Eugster, O., Marti, K., 1965. A redetermination of the isotopic composition of atmospheric neon. Z. Naturforsch. 20A, 623–624.

Eugster, O., 1988. Cosmic-ray production rates for ^{3}He, ^{21}Ne, ^{38}Ar, ^{83}Kr, and ^{126}Xe in chondrites based on ^{81}Kr-Kr exposure ages. Geochim. Cosmochim. Acta 52 (6), 1649–1662.

Gattacceca, J., Valenzuela, M., Uehara, M., Jull, A.J.T., Giscard, M.D., Rochette, P., Braucher, R., Suavet, C., Gounelle, M., Morata, D., Munayco, P., Bourot-Denise, M., Bourles, D., Demory, F., 2011. The densest meteorite collection area in hot deserts: The San Juan meteorite field (Atacama Desert, Chile). Meteorit. Planet. Sci. 46 (9), 1276–1287.

Gnos, E., Lorenzetti, S., Eugster, O., Jull, A.T., Hofmann, B.A., Al-Kathiri, A., et al., 2009. The jiddat al harasis 073 strewn field, Sultanate of Oman. Meteorit. Planet. Sci. 44 (3), 375–387.

Herzog, G.F., Caffee, M.W., 2014. Cosmic-ray exposure ages of meteorites. mcp 1, 419–454.

Huber, L., Hofmann, B., Gnos, E., 2006. The Exposure History of the JaH 073 Meteorite. LPI. 1628.

Hutson, M., Ruzicka, A., Jull, A.J.T., Smaller, J.E., Brown, R., 2013. Stones from Mohave County, Arizona: Multiple falls in the "Franconia strewn field". Meteorit. Planet. Sci. 48 (3), 365–389.

Hutzler, A., Gattacceca, J., Rochette, P., Braucher, R., Carro, B., Christensen, E., Gounelle, M., Ouazaa, N.L., Martinez, R., Valenzuela, M., Warner, M., 2016. Description of a very dense meteorite collection area in western Atacama: Insight into the long-term composition of the meteorite flux to Earth. Meteorit. Planet. Sci. 51 (3), 468–482.

Kring, D.A., Jull, A.J.T., Mchargue, L.R., Bland, P.A., Hill, D.H., Berry, F.J., 2001. Gold Basin meteorite strewn field, Mojave Desert, northwestern Arizona: Relic of a small late Pleistocene impact event. Meteorit. Planet. Sci. 36 (8), 1057–1066.

Lee, J.Y., Marti, K., Severinghaus, J.P., Kawamura, K., Yoo, H.S., et al., 2006. A redetermination of the isotopic abundances of atmospheric Ar. Geochim. Cosmochim. Acta 70, 4507–4512.

Leya, I., Masarik, J., 2009. Cosmogenic nuclides in stony meteorites revisited. Meteorit. Planet. Sci. 44, 1061–1086.

Li, S.L., Hsu, W.B., 2014. New dense meteorite collection areas were found in Lop Nur, Xinjiang. Chinese Sci. Bull. 59 (21), 2091.

Li, S.J., Wang, S.J., Leya, I., Smith, T., Tang, J., Wang, P., Zeng, X.J., Li, Y., 2017. A chondrite strewn field was found in east of Lop Nor, Xinjiang. Chinese Sci. Bull. 62 (21), 2407–2415.

Li, S.J., Wang, S.J., Miao, B.K., Li, Y., Li, X.Y., Zeng, X.J., Xia, Z.P., 2019. The density, porosity, and pore morphology of fall and find ordinary chondrites. J. Geophys. Res. Planets 124, 2945–2969.

Li, S., Luo, W., Li, B., Li, Y., 2020. The survey of Mangui meteorite shower in Xishuangbanna, Yunnan Province. Acta Mineralogica Sinica 40, 176–182. In Chinese with English abstract.

Lodders, K., Fegley, B., Lodders, F., 1998. The planetary scientist's companion. Politics.

Muñoz, C., Guerra, N., Martinez-Frias, J., Lunar, R., Cerda, J., 2007. The Atacama Desert: A preferential arid region for the recovery of meteorites—Find location features and strewnfield distribution patterns. J. Arid Environ. 71 (2), 188–200.

Nishiizumi, K., Regnier, S., Marti, K., 1980. Cosmic ray exposure ages of chondrites, pre-irradiation and constancy of cosmic ray flux in the past. Earth Planet. Sci. Lett. 50 (1), 156–170.

Ouazaa, N.L., Perchiazzi, N., Kassaa, S., Zeoli, A., Mohamed, G., et al., 2009. Meteorite finds from southern Tunisia. Meteorit. Planet. Sci. 44 (7), 955–960.

Pourkhorsandi, H., Mirnejad, H., 2013. Lut Desert (Iran): A high-potential area for finding meteorites. Meteorit. Planet. Sci. 48 (2).

Pourkhorsandi, H., Gattacceca, J., Rochett, P., D'Orazio, M., Kamali, H., De Avillez, R., et al., 2019. Meteorites from the Lut Desert (Iran). Meteorit. Planet. Sci. 54 (8), 1737–1763.

Rubin, A., Verish, R.S., Moore, C.B., et al., 2000. Numerous unpaired meteorites exposed on a deflating playa lake at Lucerne Valley, California. Meteoritics Planet. Sci. 35 (S5), A181–A183.

Schluter, J., Schultz, L., Thiedig, F., Al-Mahdi, B.O., Abu Aghreb, A.E., 2002. The Dar al Gani meteorite field (Libyan Sahara): Geological setting, pairing of meteorites, and recovery density. Meteorit. Planet. Sci. 37 (8), 1079–1093.

Simon, S.B., Wacker, J.F., Clayton, R.N., Mayeda, T.K., Schwande, J.R., Sipiera, P.P., Wacker, J.F., Wadhwa, M., 2004. The fall, recovery and classification of the Park Forest meteorite. Meteorit. Planet. Sci. 39, 625–634.

Stoffler, D., Keil, K., Scott, E.R.D., 1991. Shock metamorphism of ordinary chondrites. Geochim. Cosmochim. Acta 55 (12), 3845–3867.

Van Schmus, W.R., Wood, J.A., 1967. A chemical petrologic classification for the chondritic meteorites. Geochim. Cosmochim. Acta 81, 747–765.

Weisberg, M.K., McCoy, T.J., Krot, A.N., 2006. Systematics and evaluation of meteorite classification. Meteorites and the early solar system II.

Wlotzka, F.A., 1993. A weathering scale for the ordinary chondrites. Meteoritics 28 (28), 460.

Zeng, X., Li, S.J., Leya, I., Wang, S.J., Smith, T., Li, Y., Wang, P., 2018. The Kumtag 016 L5 strewn field, Xinjiang Province, China. Meteoritics Planet. Sci. 53, 1113–1130.

Zolensky, M.E., Wells, G.L., Rendell, H.M., 1990. The accumulation rate of meteorite falls at the Earth's surface: The view from Roosevelt County, New Mexico. Meteoritics Planet. Sci. 25 (1), 11–17.

Zhang, C.Q., Lou, D.B., Xiao, K.Y., Dong, Q.J., Ding, J.H., Wang, P., Zhang, Z.H., Qu, W.J., 2010. Geological characteristics of the kumtag molybdenum deposit and the Re-Os isotope age of the molybdenite in Hami area, Xinjiang. Geol. Bull. 29 (10), 1586–1593.

Yang, H.L., Zang, Y.G., Duo, H.R., Wang, X.L., Li, D.Q., 2012. Insect diversity in the kumtag desert. Scientia Silvae Sinicae 48 (09), 176–180.

Joint investigation group of "Jilin meteorite rain"., 1977. Preliminary investigation of jilin meteorite rain. Science China. (01):38-45+93-94.